A NONDESTRUCTIVE METHOD FOR CHARACTERIZATION OF ONE DIMENSIONAL PERMEABILITY DISTRIBUTION AT THE CORE SCALE

A. Soltani[1], M. Le Ravalec-Dupin[1], M. Fourar[2] and P. Egermann[1]
[1] Reservoir Engineering Department, Institut Français du Pétrole, France
[2] LEMTA, Ecole des Mines de Nancy, France

This paper was prepared for presentation at the International Symposium of the Society of Core Analysts held in Calgary, Canada, 10-12 September, 2007

ABSTRACT

Many reservoir simulator inputs are derived from laboratory experiments. Special core analysis techniques generally assume that core samples are homogeneous. This assumption does not hold for porous media with significant heterogeneities. This paper presents a new method to characterize core scale permeability heterogeneity. This method is validated by both numerical and experimental results.
The leading idea consists in injecting a high viscosity miscible fluid into a core sample saturated by a low viscosity fluid. In such conditions, the fluid displacement is expected to be piston-like. We investigate the evolution of the pressure drop as a function of time. A continuous permeability profile is estimated along the flow direction from an interpretation technique where the core sample is assumed to be a stack of infinitely thin cross-sections perpendicular to the main flow direction. Thus, we determine a permeability value for each cross-section.
Numerical and laboratory experiments are performed in order to validate the method. Flow simulations are performed for numerical models representing core samples to estimate the pressure drop. The selected models are sequences of plugs with constant permeabilities. In addition, laboratory displacements are conducted for both low permeable and high permeable core samples. To investigate whether there is diffusion inside the porous medium, CT-scan measurements are performed during fluid displacement: the location of the front is observed at successive time intervals. The results validate the methodology developed in this paper as long as heterogeneity is one-dimensional.

INTRODUCTION

Experiments provide data at the core scale, which are processed to estimate a given property, assuming the core sample is homogeneous. This assumption clearly makes post-processing easier, but may be inappropriate. For instance, laboratory experiments for measuring relative permeability are often unsteady-state, because they are quicker than steady-state experiments. The drawback is that the flow functions are indirectly inferred from the measurements. The interpretation process relies on the Buckley-Leverett method (Buckley and Leverett, 1942; Welge, 1952) and the JBN method (Johnson *et al*., 1959), for which the core is assumed to be homogeneous and isotropic. Recent studies show that the validity of such assumptions can be questioned (Valestrand, 1999). In this paper, we

aim at developing a physical approach to directly assess permeability heterogeneity at the core scale. The leading idea consists in injecting a high viscosity miscible fluid into a core sample saturated by a low viscosity fluid. Fluid displacement is expected to be piston-like. The variations in pressure drop across the core are monitored during injection. In the first section, we introduce a procedure for deriving the permeability profile along the flow direction axis from the pressure drop. Then, in the second and third sections, we validate this methodology from numerical and laboratory experiments.

DESCRIPTION OF THE METHODOLOGY

Our method is inspired by the work of Fincham and Gouth (2000). However, in this paper we focus on the characterization of the profile of the absolute permeabilities instead of the relative permeabilities. Therefore, we consider the injection of a high viscosity miscible fluid into a core sample initially saturated by a low viscosity fluid. We assume that the two fluids are incompressible and that temperature is constant (*i.e.*, porosity, densities and viscosities are constants). The high viscosity fluid is injected through one end of the core ($x = 0$) at constant filtration velocity. The escaping fluids are collected at the other end ($x = L$) at atmospheric pressure. The pressure drop across the core, $\Delta p = p_{inlet} - p_{outlet}$ is measured as a function of time. The following assumptions are made:

1. The fluid movement is dominated by viscous forces. The displacement is miscible: there is no capillary pressure effect.
2. The displacing front in the sample is assumed to be sharp (due to high viscosity ratio).
3. The absolute permeabilities of the core sample for both invading and defending fluids are the same.

Considering the one dimensional flow of a single-phase fluid through a porous medium, the differential form of Darcy's law (1856) is:

$$Q = \frac{kA}{\mu} \times \frac{dp}{dx} \tag{1}$$

Q is the flow rate, k the absolute permeability, A the cross sectional area of the core sample, μ the viscosity of the invading fluid, p the pressure and x is the coordinate axis along the flow direction. This law states that for a strictly homogeneous core sample, there is a linear relationship between flow rate and pressure drop, whose slope provides the permeability k.

The viscous displacement considered here is unsteady-state, which means that the pressure drop along the medium is a function of time. The integration of the above equation with respect to any location x gives:

$$\Delta p(t) = \int_0^x \frac{Q\mu}{Ak(x)} dx \tag{2}$$

In Equation (2), permeability k is the only variable depending on x. If we assume that the displacement is piston-like and x is the front location inside the porous medium, then the pressure drop across the core can be written as the sum of the pressure drop in the invading fluid (high viscosity fluid) and the pressure drop in the defending fluid (low

viscosity fluid):

$$\Delta p_{inlet-outlet} = \Delta p(t) = \Delta p_{inlet-front} + \Delta p_{front-outlet} \tag{3}$$

Rewriting Equation (2) for the invading and defending fluid pressure drops and substituting the results in Equation (3) leads to:

$$\Delta p(t) = \int_0^{x_f} \frac{Q\mu_{invading}}{Ak(x)}\,dx + \int_{x_f}^{L} \frac{Q\mu_{defending}}{Ak(x)}\,dx \tag{4}$$

where x_f is the front location. The Buckley-Leverett frontal theory (Buckley and Leverett, 1942) was developed for dealing with steep fronts. Its concept provides the following relationship between front location and time:

$$x_f = \frac{Q}{A\phi}t \tag{5}$$

ϕ is the porosity. As shown above, the absolute permeability is a function of front location. Referring to Equation **(5)**, it is also a function of time. We compute the time derivatives of both sides of equation (4):

$$\frac{\partial \Delta p(t)}{\partial dt} = \frac{Q}{A\phi}\left(\frac{Q\mu_{invading}}{Ak(x_f)} - \frac{Q\mu_{defending}}{Ak(x_f)}\right) \tag{6}$$

Therefore, we obtain the following formulation for $k(x_f)$:

$$k(x_f) = k = \frac{Q^2\left(\mu_{invading} - \mu_{defending}\right)}{A^2\phi\dfrac{\partial \Delta p(t)}{\partial t}} \tag{7}$$

We thus obtain the variation in k along the flow direction when the steep front moves inside the porous medium. As the front location is a function of time, we can deduce the permeability profile versus injection time.

NUMERICAL VALIDATION

In this section, we perform numerical tests to validate our methodology. Flow simulations are performed using a streamline simulator. We consider two numerical models, which represent two composite cores created from four homogeneous plugs butted together. The petrophysical properties of these plugs are reported in Table 1. The two models, named Model-1 and Model-2, are built on 3D grids with 124800 grid blocks ($78\times40\times40$). Such dimensions are selected to be consistent with the plugs used in the laboratory (see the following section). We first simulate immiscible displacements ignoring molecular diffusion and irreducible water saturation. Then, we simulate miscible displacements to assess the impact of molecular diffusion and see how diffusion can affect the determination of the permeability profile. In both cases, a direct line drive pattern is used (the injection period is about 1.5 hours). We consider conditions identical to those of our laboratory experiments (see the following section) and choose relative permeability curves that ensure a piston-like displacement. The conditions are:

1. Slightly heterogeneous permeability fields are generated to populate plugs. We check that the average permeabilities of plugs equal their absolute permeabilities measured in the laboratory (Table 1). Porosity is constant per plug. It also respects the values measured in the laboratory (Table 1)
2. We use straight line relative permeability curves with end points of 1, *i.e.*, $k_{rw} = S_w$ and $k_{ro} = 1\text{-}S_w$. Therefore, $k_{rw}+k_{ro} = 1$ whatever S_w.
3. The mobility (or viscosity) ratio is very favorable ($M>>1$).
4. There is no capillary effect.

For stable miscible displacements, convection should control dispersion. The results of tracer tests are usually used to determine convenient flow rates. However, Fourar *et al*. (2005) showed that for heterogeneous core samples, the effluent concentration profiles do not depend on flow rates and molecular diffusion can be ignored. Thus, our numerical simulations are performed with flow rates, which correspond to the optimal flow rate allowed by our laboratory devices (core holder and pressure transducers).

Numerical Immiscible Displacement

After a series of sensitivity tests, the viscosity ratio ($\mu_{invading} / \mu_{defending}$) is set to 60, the gravity effects are ignored and the minimum number of time-steps is set to 100. During the numerical simulation, the injected fluid invades the plugs one after the other. The numerical simulation provides pressure and saturation data for all grid blocks at different time steps. For each time step, the inlet and outlet faces pressure drop is calculated using Equation (8):

$$\Delta p(t) = \frac{\sum_{1}^{N_z \times N_y} p_{inlet-face}}{N_z \times N_y} - \frac{\sum_{1}^{N_z \times N_y} p_{outlet-face}}{N_z \times N_y} \tag{8}$$

N_y and N_z are the number of grid blocks along axes y and z. The methodology presented in the first section is applied to derive the permeability variations along the flow direction axis from the simulated pressure drop. The numerical pressure drops are plotted for both Model-1 and Model-2 in Figure 1 (top). The $\Delta p(t)$ behavior clearly shows the existence of four different areas in both models. The 2D view of the saturation map (Figure 1, bottom) shows a sharp front at different time steps. The processed results are compared to the actual permeabilities of the two models in

Figure 2. We check that the permeabilities derived from our methodology duplicate the actual permeabilities of the plugs. The result of our 1D permeability mapping technique shows a perfect match with the absolute permeability of the selected plugs.

Numerical Miscible Displacement

We also simulate miscible displacements to investigate the influence of miscibility on the pressure drop. We assume that 10% of the invading phase components dissolve into the defending phase, which results in the creation of a mixed zone. The mixed zone viscosity is calculated using a quarter-power mixing rule (Sahimi, 1995). Miscible displacements

are simulated for the two models described above with flow conditions identical to those of the immiscible case. Figure 3 (top) shows the numerical pressure drops and 2D view of the saturation maps (bottom) for two models. The front remains sharp and dispersion is still negligible. Because of the mixing zone in between the invading and defending fluids, the pressure changes get smoother and the limits between the plugs are less obvious. Applying the methodology presented in the first section leads to smoothed permeability profiles (Figure 4). However, a strong agreement is still observed between the actual and estimated permeabilities.

EXPERIMENTAL VALIDATION

We use an experimental device thought up to conduct steady and unsteady state flow experiments in consolidated core samples submitted to room or high pressures and temperatures. The core holder is designed so that the pressure drop is monitored as a function of time. X-ray scan images are collected at different times and are interpreted in terms of concentrations. The selected valves make it possible to simultaneously measure different properties (*e.g.*, fluid temperature, fluid conductivity, inlet-outlet resistivity, *etc*.).

Core Selection

During the experiments, we handle two types of samples: two artificially heterogeneous samples built from plugs butted together and three truly heterogeneous samples.

To build the artificially heterogeneous samples, we selected several sandstone and limestone samples of 38 mm diameter and up to 80 mm length. We only kept the ones considered as homogeneous, that is those whose CT adsorption profiles were roughly constant along axis X. Then, plugs were extracted from these samples and butted together to create two heterogeneous core samples (

Figure 5). The petrophysical properties of these plugs are reported in Table 1. The two resulting samples correspond to the two numerical models considered when performing the numerical experiments.

The three heterogeneous samples are heterogeneous at scales much larger than the pore scale. They consist of (1) a low permeability limestone with a thick shale layer, (2) a high permeability limestone with local porosity alteration due to acidification, and (3) a friable coarse-grained sandstone containing lots of mica and clay minerals and a thick visible layer in the middle whose nature is unknown. Their porosities and permeabilities were measured prior to any experiment. Then, the injection of the high viscosity fluid starts and the pressure drop is monitored while concentration maps are collected at successive times. In the following section, we present the results of our interpretation technique to derive the permeability profile from the pressure drop.

Experimental Results

Composite Samples

We proceed as follows: the two artificially heterogeneous samples are initially saturated by a 30% *NaCl* brine at room temperature. The initial pressure is uniform and assumed to be 10^5 Pascal. Strong core-holders jacket the circumference boundary of the composites (and other core samples) so that flow is linear with no-flow boundary conditions. Then, a

60 cp glycerin-brine mixture is injected at a constant flow rate of 15 cc/hr. The pressure drop is recorded until stabilization.
The CT-scan measurements collected for composite 2 are reported in Figure 6. They confirm that the assumption relative to the sharpness of the front is reasonable. The permeability profiles determined from our procedure are compared to the actual permeabilities of the plugs used to build composites 1 and 2 in Figure 7. The agreement is not as good as pointed out for the numerical experiments, but is still of interest. The dead volume inside the inlet port and spiral of the core holder was not purged to facilitate the identification of the pressure base line. However, the mixing of the dead volume and glycerin produces some high permeability values at the beginning of our estimated permeability profiles.
Some remarks can be emphasized. First: the higher the permeability, the stronger the noise in the estimation. This behavior is expected because the pressure drop is inversely proportional to permeability. Second: at the beginning of the displacement, the recorded $\Delta p(t)$ varies slowly due to mixing of brine dead volume and glycerin. After a while, a complete invading phase forms and progresses inside the medium. After breakthrough, the brine is still produced during several minutes (long-time tail concentration profile) but recorded $\Delta p(t)$ varies very slowly. The small variations in $\Delta p(t)$ at the beginning and end of experiment explain why our method does not succeed in estimating the permeability at two ends of our samples (Figure 7). An inverse injection at the same conditions can help to minimize this error. Third: the permeability jumps from one plug to another one are not as sharp as for the numerical experiments. This behavior, also pointed out when simulating miscible displacements, is related to the miscibility of the fluids. There is a transition zone between the invading and defending fluids, which produces a smoothing effect.

Low Permeability Limestone Sample

We now consider a heterogeneous limestone sample. Its absolute permeability is 4.0 mD. The CT profile (Figure 8, left) measured for this sample shows two distinct regions. The high viscosity fluid is injected at a flow rate of 6 cc/hr. Once the miscible displacement is over, the sample is cut into two plugs based on the observed sharp change in its CT-scan profile. Then, we measure the absolute permeability of each plug. Figure 8 (right) shows that there is a good agreement between the processed permeability profile and the absolute permeabilities of the plugs. As it was stated for composite samples, the permeability values cannot be perfectly estimated at the beginning and end of the displacement.

High Permeability Limestone Sample

The second truly heterogeneous sample is a limestone with a permeability of 240 mD. Its heterogeneity was primarily enhanced through a CO_2 injection: heterogeneity occurs along the flow axis, but also in cross-sections (Figure 9, left). For this sample, we perform two injection experiments both with flow rate of 30 cc/hr: one from left to right, which allows for capturing the permeability profile in the first half of the sample and one from right to left, which allows for capturing the permeability profile in the second half.

The inverse injection is preferred whenever the sample permeability is high. Thus, we hope to overcome first, the front spreading and second, the difficulties related to the noise intrinsic to the estimation of high permeability values. For comparison purposes, 32 minipermeameters were located along the core. They yield a mean surface permeability for 8 cross-sections. Results are reported in Figure 9 (right) and again they stress the capabilities of the methodology proposed in this paper.

Permeable Coarse-Grained Sandstone

The third heterogeneous sample is a coarse-grained sandstone with an absolute permeability of 170 mD. It contains a distinct layer of about 1.5 cm width, whose nature is not clearly identified. Small scale heterogeneity is also evidenced when looking at the sample CT profile. X-ray imaging was primarily performed during a tracer test in order to better capture the impact of heterogeneity. The collected images point out a very disperse front (Figure 10, top). No stratification or barrier to flow is clearly observed. CT images measured during a first viscous displacement (flow rate: 60 cc/hr) showed again that the front rapidly disperses. As a result, we increased the viscosity of glycerin to 200 cp and ran again the experiment. In such conditions, the front is more stable. However, Figure 10 (bottom) shows that the front is not sharp enough. The pressure drop is measured when the fluid is injected from left to right and from right to left. Then, these data are processed to estimate the 1D permeability profile (Figure 11). Permeability varies between 70 and 220 mD. As the sample is friable, no other measurement could be collected to crosscheck our results.

CONCLUSIONS AND PERSPECTIVES

This paper presents a methodology for characterizing the permeability profile in cores along the flow direction axis. It involves the injection of a high viscosity miscible fluid into a core sample initially saturated by a low viscosity fluid. We derived the permeability profile from the variations in the pressure drop across the core.

This methodology was validated through numerical experiments. Flow simulations were performed for numerical models representing core samples. The models studied were sequences of plugs with given mean permeabilities. We simulated the pressure drop between the inlet and outlet faces considering both miscible and immiscible fluids. The interpretation procedure provided the expected permeability profile. However, we pointed out a smoothing effect in the case of miscible fluids, which is due to the mixing zone between the invading and defending fluids.

The methodology was also validated by laboratory experiments. The process works well for low permeabilities. In the case of permeable samples, as the pressure drop is inversely proportional to permeability, the estimated permeabilities are very noisy. The determination of the permeability profile was improved by performing an injection in one direction and another one in the reverse direction.

The analysis of the results obtained for the truly heterogeneous cores pointed out another difficulty. The proposed methodology assumes that permeability is homogeneous per cross-section, which means that heterogeneity is one dimensional. Our ongoing research focuses on the development of new procedures able to capture 3D heterogeneity.

NOMENCLATURE

Δp	Pressure drop	k_{ro}	Oil relative permeability
x	Location	ρ	Density
k	permeability (field)	CT	Computer tomography
A	Cross sectional area	N_y	Number of grid-blocks in y direction
μ	Viscosity	N_z	Number of grid-blocks in z direction
Q	Flow rate	M	Mobility ration
t	Time	x_f	Front location
S_w	Water saturation	ϕ	Porosity (field)
k_{rw}	Water relative permeability		

REFERENCES

[1] Buckley, S.E. and Leverett, M.C., Mechanisms of fluid displacement in sands, *Trans. Am. Inst. Min. Eng.*, (1942) **146**, 107-116.

[2] Darcy, H., *Les fontaines publiques de la ville de Dijon*, Victor Dalmont, Paris, France, (1856).

[3] Fincham, A. and Gouth, F., Improvements of core flooding design and interpretation using a new software, *Society of Core Analysts Symposium*, Abu Dhabi, 9-12 October (2000).

[4] Fourar M., Konan G., Fichen C., Rosenberg E., Egermann P. and Lenormand R., Tracer Tests for Various Carbonate Cores Using X-ray CT, SCA paper 2005-56, Toronto, Canada (2005).

[5] Johnson, E.F., Bossler, D.P. and Naumann, V.O., Calculation of relative permeability from displacement experiments, *Trans. Am. Inst. Min. Eng.* (1959) **216**, 370-372.

[6] Sahimi Muhammad, *Flow and Transport in Porous Media and Fractured Rock*: VCH, Germany, (1995).

[7] Valestrand, R., The impact of permeability heterogeneities on flow function estimation,
Cand. Scient. Thesis in Physics, Dept. of Physics, Univ. of Bergen, Norway (1999).

[8] Welge, H.J., A simplified method for computing oil recovery by gas or water drive, *Trans. Am. Inst. Min. Eng.* (1952) **195**, 91-98.

AKNOWLEDGEMENTS

We would like to thank our colleagues from department of core analysis (IFP) who gave us the opportunity to perform our experiments. Our special thanks to J.Marc Lombard, Elisabeth Resenberg, Corinne Fichen and Herve Deshamps for their helps and supports.

Table 1. Physical and petrophysical properties of different plugs. These plugs, butted together, are used to create numerical and laboratory samples.

			Physical and Pertophysical Properties			
			Length (cm)	Diameter (cm)	Permeability (mD)	Porosity (%)
Model-1	Laboratory Sample Name	GDV	1.82	3.80	70	17
		Lavoux	1.78	3.77	3	25
		Brauvillier	1.84	3.79	29	27
		M3858	1.80	3.78	62	22
Model-2	Laboratory Sample Name	GDV	1.82	3.80	70	17
		LavouxII	1.78	3.78	4.5	24
		GDF	1.78	3.78	106	9
		V5-1	1.78	3.78	62	23

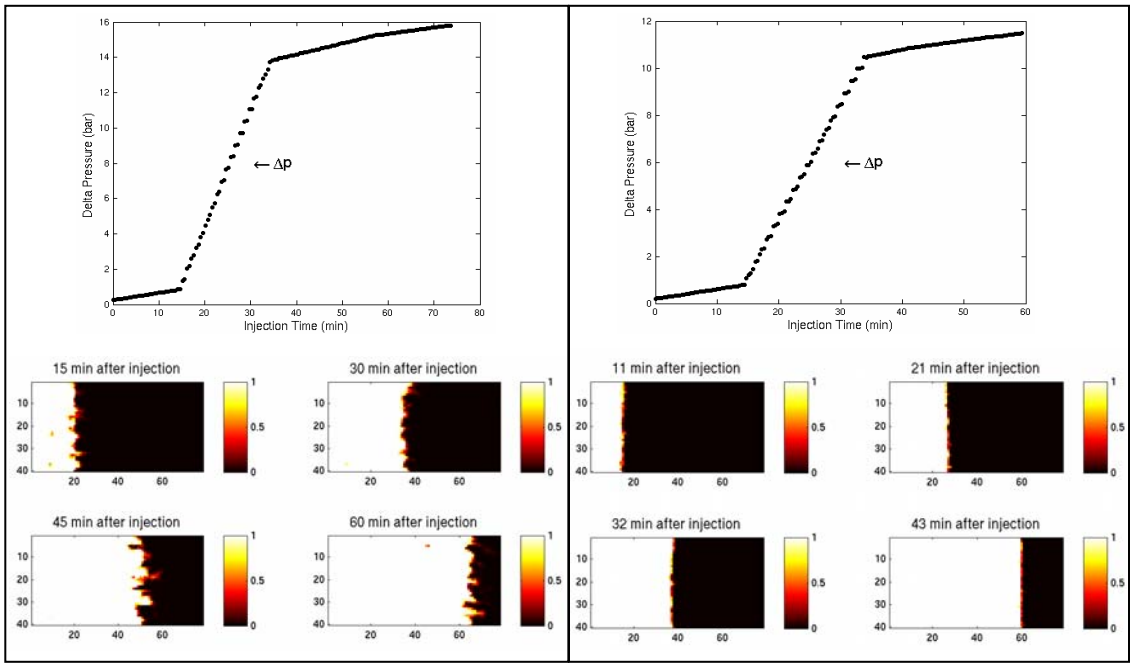

Figure 1. Top: Numerical pressure drop of Model-1 (left) and Model-2 (right) when performing immiscible displacement. Bottom: 2D view of front displacement inside Model-1 (left) and Model-2 (right). The color bars show the invading fluid saturation.

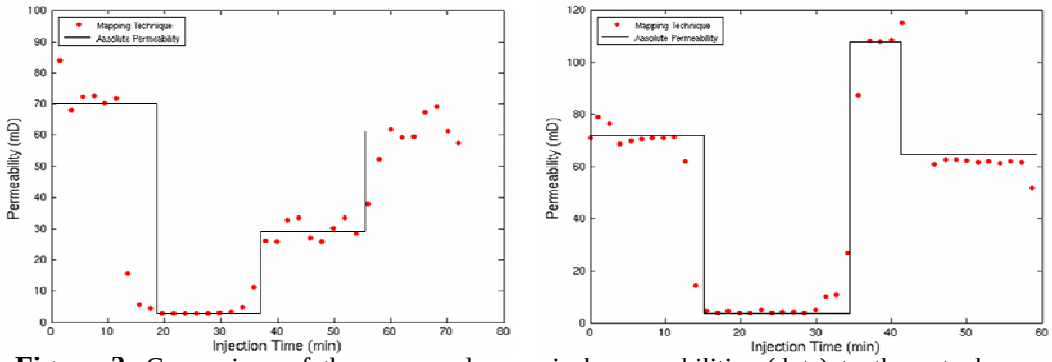

Figure 2. Comparison of the processed numerical permeabilities (dots) to the actual ones (lines) for Model-1 (left) and Model-2 (right) when performing immiscible displacement.

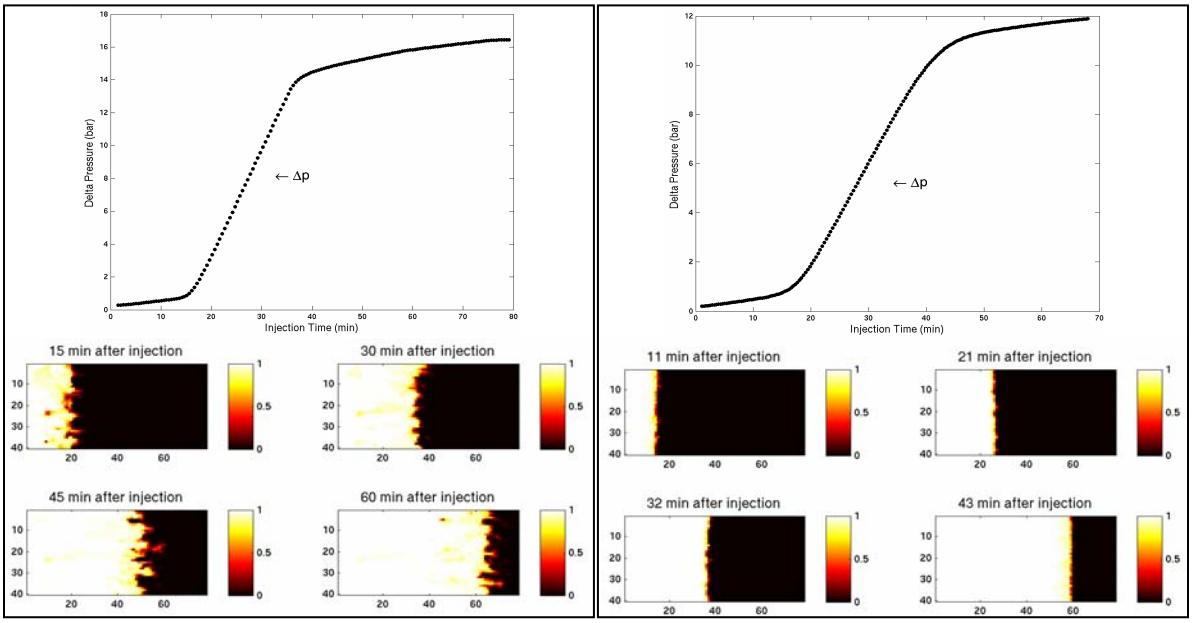

Figure 3. Top: Numerical pressure drop of Model-1 (left) and Model-2 (right) when performing miscible displacement. Bottom: 2D view of front displacement inside Model-1 (left) and Model-2 (right). The color bars show the invading fluid saturation.

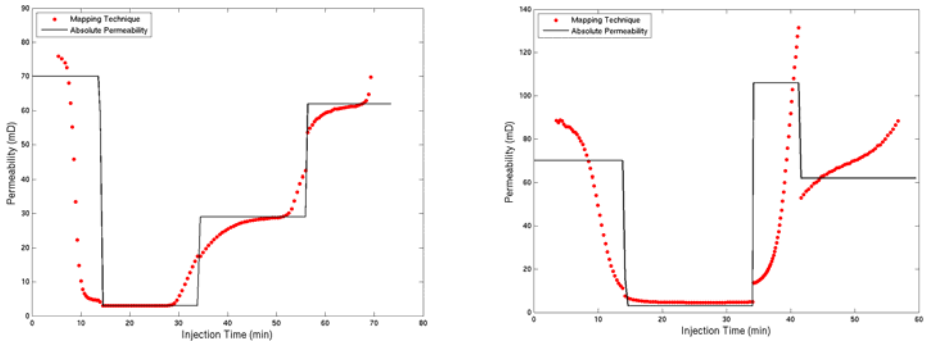

Figure 4. Comparison of the processed numerical permeabilities (dots) to the actual ones (lines) for Model-1 (left) and Model-2 (right) when performing miscible displacement.

Figure 5. Composite 1 (left) and composite 2 (right) which represent longitudinal heterogeneity along the sample.

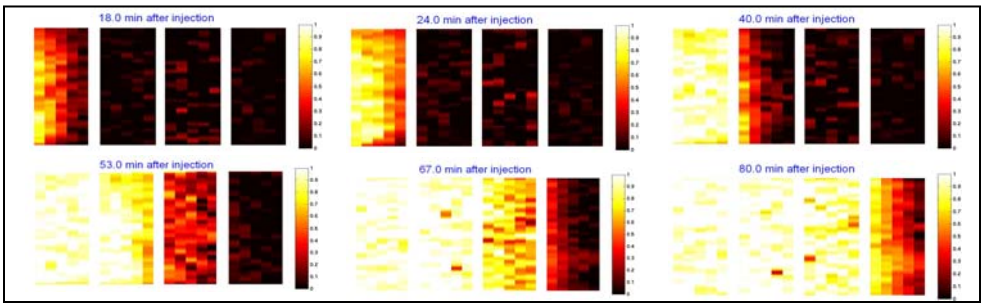

Figure 6. 2D maps of the concentration of the injected glycerin at successive times for composite 2. Four small plugs are separated for a better observation. The color bars show the invading fluid concentration.

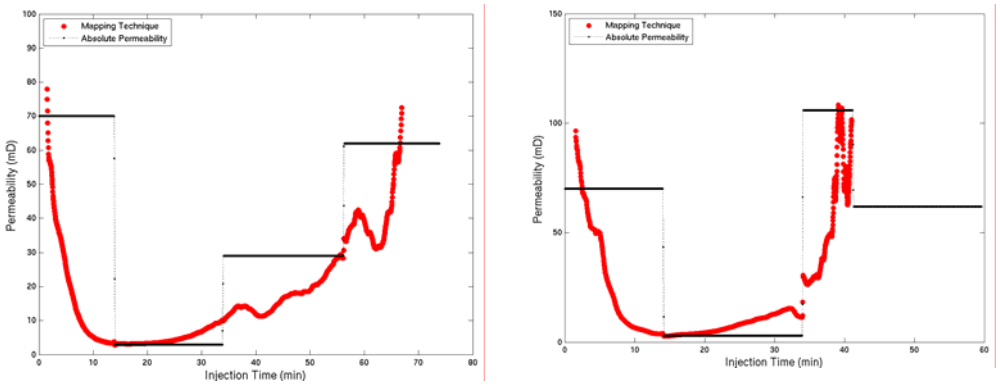

Figure 7. Comparison of the processed experimental permeabilities (dots) to the actual ones (lines) for composite 1 (left) and composite 2 (right) when performing viscous miscible displacement.

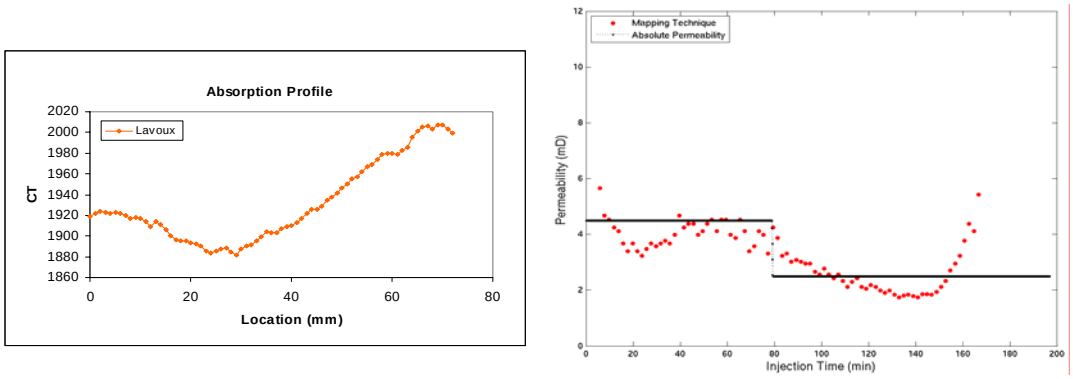

Figure 8. Left: Low permeability limestone sample CT profile. Right: Comparison of the processed permeabilities (dots) to the actual ones (lines) for this sample.

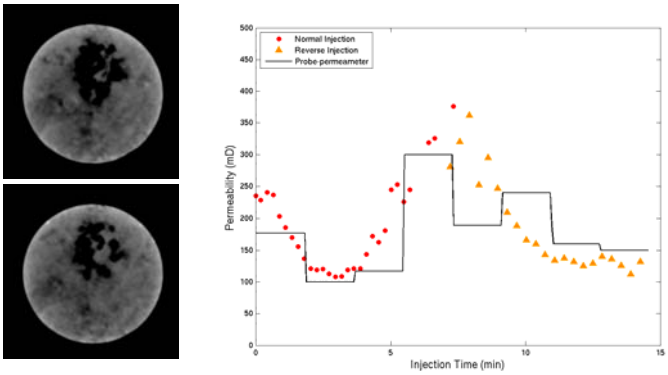

Figure 9. Left: cross sectional X-ray images of permeable limestone sample taken at 5 (top) and 8 mm (bottom) distance from inlet face. Right: comparison of processed permeabilities (dots and triangles) to the minipermeameter results (lines). Dots indicate that the injection is performed from left to right and triangles from right to left.

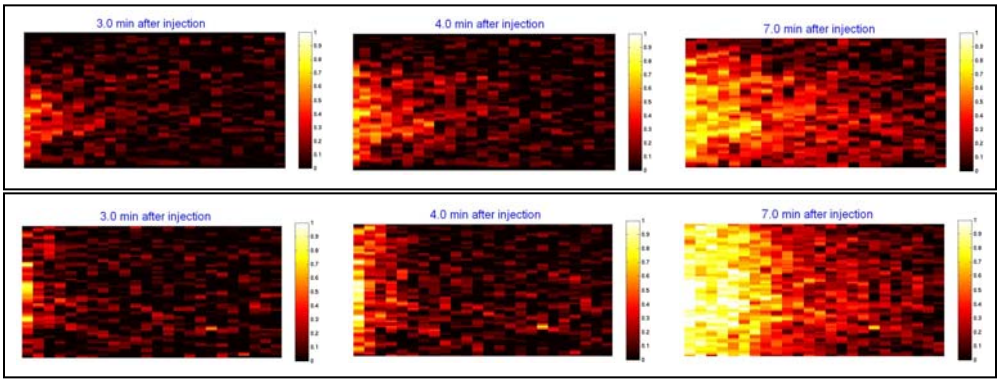

Figure 10. 2D maps of the concentration of the injected fluid at successive times for coarse-grained sandstone sample. Top: tracer displacement. Bottom: viscous displacement. The color bars show the invading fluid (glycerin-brine mixture) concentration.

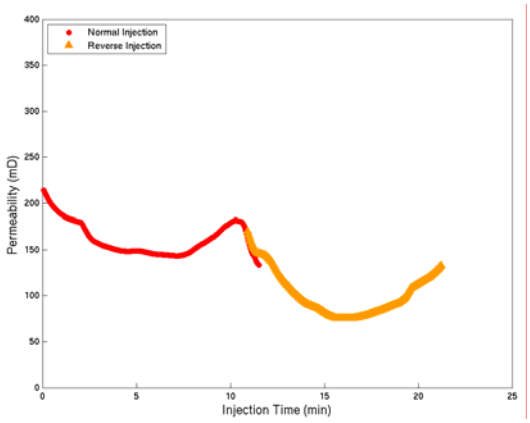

Figure 11. The processed permeabilities (dots and triangles) of high permeable coarse-grained sandstone. Dots indicate that the injection is performed from left to right and triangles from right to left.